Polygon-Shaped Slotted Dual-Band Antenna for Wearable Applications

Esther Florence Sundarsingh, Sangeetha Velan, Malathi Kanagasabai, *Member, IEEE*, Aswathy K. Sarma, Chinnambeti Raviteja, and M. Gulam Nabi Alsath

***Abstract*—This letter presents the design of a wearable dual-band patch antenna for operating in the GSM-900 and 1800 bands. The proposed polygon patch antenna comprises a circular slot and vertical slits embedded on jeans substrate. This structure provides two paths for currents, making it viable for dual bands. The effect of patch length, slot radius, and slit length on the overall antenna performance is analyzed by performing a comprehensive parametric study. Further bending, crumpling, wetness, and on-body measurements have been performed to validate the structure. Specific absorption rate (SAR) values ranging between 0.00039–0.0035 W/Kg have been obtained for two different analyses.**

***Index Terms*—Body area network (BAN), dual-band, specific absorption rate (SAR), wearable antenna.**

I. Introduction

IN RECENT days, there is an extensive focus on personal area network (PAN), more precisely on body area network (BAN). This is evident from the advent of wearable biosensors, cameras, computers, fitness devices and several other wearable gadgets. Such developments kindle a natural interest in the emergence and growth of wearable antenna, an antenna embedded as a part of our clothing.

Different textile materials and polymers have been proposed to be used as flexible substrates [1]–[4]. In this letter, the dual-band antenna has been designed on jeans fabric [4], which is flexible to suit the human body. It has low dielectric constant, which provides improved radiation.

In wearable domain, dual-band is reported in finger ring antennas, [5]. However, coupling between fingers degrades the performance. In [6], dual-band is reported in button antennas. It is a multilayered structure that requires intricate fabrication. It also creates an omnidirectional radiation pattern, causing electric and magnetic fields to penetrate into the human body. To overcome such drawbacks, in this letter, a patch antenna has been chosen because of its simple two-dimensional geometry that makes it inexpensive and easy to fabricate. The ground plane eliminates the absorption of radiation into the human body. Considerable directivity is also obtained in the required bands. The proposed design can easily be attached to the fabric, either on the torso or on the back of a person. On-body propagation measurement using a microstrip patch antenna and transient measurement of radio channels for BAN and PAN has been presented in [7] and [8]. The seed for the proposed structure has been referenced from [9] and [10]. The antenna has been designed to operate within the two mobile frequency bands, GSM-900 and GSM-1800.

In the wearable BAN (WBAN) applications, it is not always feasible to keep the antenna in a flat position. It becomes necessary to evaluate its performance under bending conditions. The textile antenna must withstand such bending stresses while maintaining its radiation specifications. The bending effect has been analyzed in [2], [11], and [12]. In practical situations, as the person takes up different positions, the antenna is more likely to get crumpled near the joints [13]. In this letter, the performance of the antenna has been measured under different bending and crumpling conditions.

Apart from bending and crumpling, wetness is another major factor that affects the antenna performance. The presence of water with high dielectric constant strongly influences the relative permittivity of the substrate. Wetness measurement has also been carried out in this letter.

The design of the antenna is explained in Section II. The effect of patch length, slot radius, and slit length on the antenna's performance is also explained in this section. The results and the discussions are presented in Section III.

II. Antenna Design

The patch antenna consists of a substrate located in between ground plane and patch. The material used for ground plane and patch is copper. The substrate is jeans fabric that has a thickness of 1 mm, dielectric constant, $\varepsilon_{\mathrm{r}} = 1.7$, and loss tangent $\delta = 0.025$ [4].

Initially, patch length $a(\lambda_{\mathrm{g}}/2)$ is computed using the standard length and width expression of a square patch, given in [14], where λ_{g} is the guided wavelength at 900 MHz. Applying the value of the lower resonant frequency $f_2 = 900$ MHz, a is obtained approximately as 128 mm. This shape is then transformed into a hexagon by cutting out portions in the corners, based on the Pythagoras theorem, to reduce the patch area. To introduce another band in the same structure, a ring-shaped slot with radius r and slot width $\lambda_0/80$ (4 mm) is introduced in the center, where λ_0 is the free-space wavelength at 900 MHz. A slit of length s is introduced in the top and bottom edges of the hexagon. This is done to increase the electrical length and to excite the fundamental-mode surface current path of the patch.

Manuscript received October 11, 2013; revised January 16, 2014; accepted March 18, 2014. Date of publication March 21, 2014; date of current version April 09, 2014.

E. F. Sundarsingh is with the Department of Electronics and Communication Engineering, SSN College of Engineering, Kalavakkam 603110, India (e-mail: estherflorences@ssn.edu.in).

S. Velan, M. Kanagasabai, A. K. Sarma, C. Raviteja, and M. G. N. Alsath are with the Department of Electronics and Communication Engineering, College of Engineering, Anna University, Chennai 600025, India (e-mail: vsangeethavelan@gmail.com; mala@annauniv.edu; aswathyksarma@gmail.com; chinnambeti.raviteja@gmail.com; mail.alsath@yahoo.com).

Color versions of one or more of the figures in this letter are available online at http://ieeexplore.ieee.org.

Digital Object Identifier 10.1109/LAWP.2014.2313133

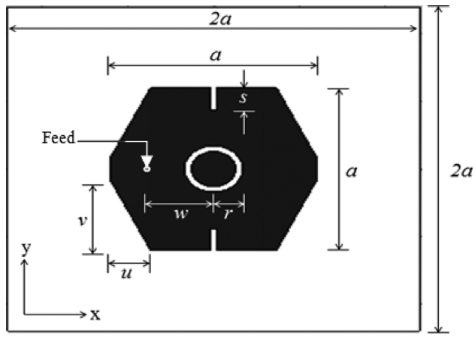

Fig. 1. Final structure dimensions: $a = 120$ mm, $r = 17$ mm, $s = 16$ mm, $u = 25$ mm, $v = 50$ mm, $w = 45$ mm.

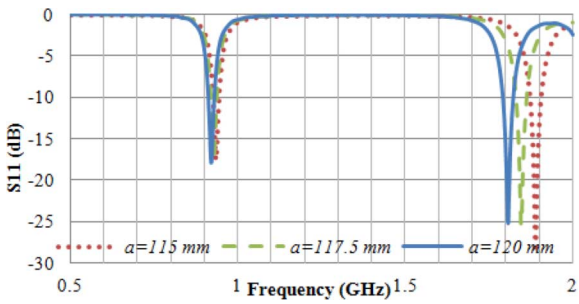

Fig. 2. S_{11} at $a = 115$, 117.5, and 120 mm. $r = 17$ mm, and $s = 16$ mm.

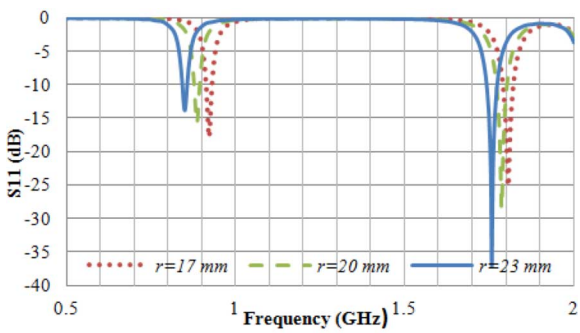

Fig. 3. S_{11} at $r = 17$, 21, and 23 mm. $a = 120$ mm, and $s = 16$ mm.

The required dual-band operation is obtained when $a = 120$ mm, $r = 17$ mm, and $s = 16$ mm. The width of both circular slot and vertical slit is $\lambda_0/80$ (4 mm). The 50-Ω feed is located in a point where perfect impedance matching is obtained for both the bands. The ground plane and substrate have the same dimensions. Each is a square of length $2a$. The dimension of the final design is illustrated in Fig. 1.

The effect of each parameter (a, r, and s) on the overall S_{11} response is illustrated in the graphs in Figs. 2–4. The dimensions a and r affect the electrical lengths at both the lower and upper resonant frequencies. Henceforth, in Figs. 2 and 3, it can be observed that when these two parameters are varied, there is a shift in both the frequency bands. By varying the length of the slit, there can be an independent control on the lower frequency band without much variation in the higher frequency band, as shown in Fig. 4.

This effect can be validated by observing the surface current distributions at 900 and 1800 MHz shown in Fig. 5. While focusing on the region surrounding the slits present in the top and bottom edges of the polygon, dense current distribution surrounding the slit is observed only in Fig. 5(a), i.e., in 900 MHz.

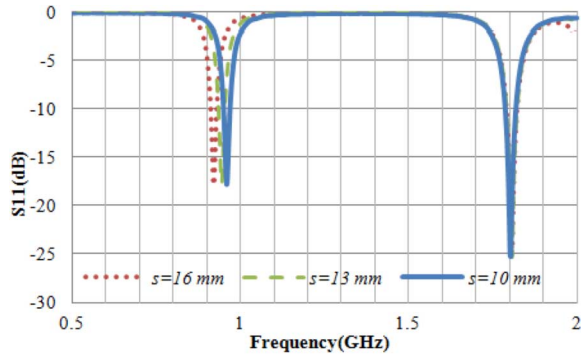

Fig. 4. S_{11} responses at $s = 16$, 13, and 10 mm. $a = 120$ mm, and $r = 17$ mm.

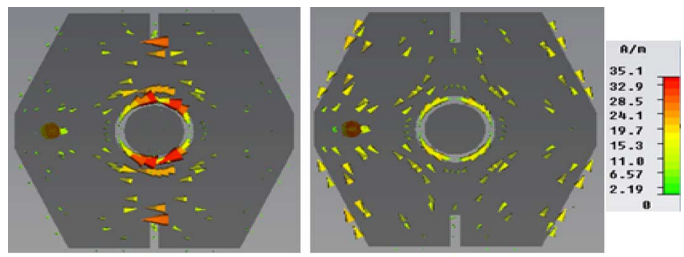

Fig. 5. (a) Surface currents at 900 MHz. (b) Surface currents at 1800 MHz.

TABLE I
FREQUENCY DETUNING FOR VARIOUS PARAMETERS

PARAMETERS		FREQUENCY DETUNING(%) 900 MHz	FREQUENCY DETUNING(%) 1800 MHz
Length of the patch a (mm)	115	4.02	5.01
	117.5	3.22	2.61
	120	2.22	0.41
Outer radius of the slot r (mm)	17	2.22	0.41
	20	1.57	0.79
	23	5.58	2.39
Length of the slit s (mm)	10	6.62	0.21
	13	4.62	0.31
	16	2.22	0.41

However in Fig. 5(b), i.e., in 1800 MHz, there is sparse current distribution in that region.

The frequency detuning for various parameters keeping 900 and 1800 MHz as the base reference is summarized in Table I.

III. Results and Discussion

The antenna is made using copper sheets and jeans fabric. The photograph of the handmade prototype is given in Fig. 6.

The designed antenna is tested using a vector network analyzer (VNA). The simulated and measured S_{11} plots for free space and on-body measurements are shown in Fig. 7. Both the patch and the substrate have been cut and glued manually. Moreover, feeding cable losses were not considered in simulation. These may be the reasons that could be attributed for the discrepancy observed between simulated and measured results.

The directivity values at higher and lower resonant frequencies are 8.1 and 7.4 dBi, respectively. The corresponding radiation (total) efficiencies are 20.5% (16.7%) and 10.3% (4.7%). The azimuth and elevation patterns at the two frequencies can be observed in Fig. 8.

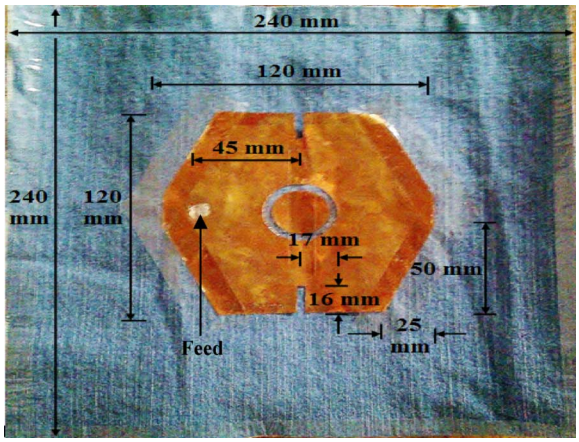

Fig. 6. Fabricated prototype of the proposed dual-band antenna.

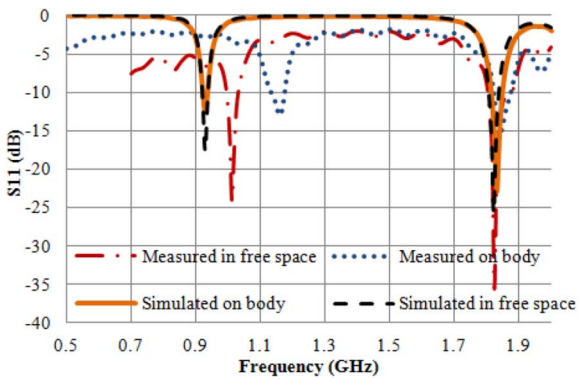

Fig. 7. Simulated and measured (free space and on-body) S_{11} response. $a = 120$ mm, $r = 17$ mm, $s = 16$ mm.

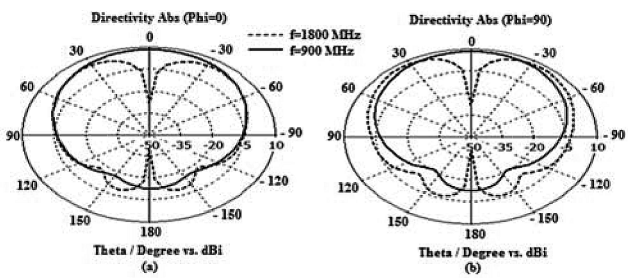

Fig. 8. Simulated far-field pattern: (a) E-plane pattern and (b) H-plane pattern.

The bending is performed by keeping the prototype around a foam cylinder of varying diameter. The effect of bending is measured in both x- and y-planes and plotted in Figs. 9 and 10. Both the bands get shifted as the bending increases in x-direction. In y-plane bending, lower band shift is much less as compared to the upper. Effect of bending can be reduced by using electromagnetic band-gap (EBG) structures [2].

Different crumpling effects have been performed on the antenna as shown in Fig. 11. It is clear from Fig. 12 that measured results show a slight shift in the upper band, whereas the lower band is getting shifted to the left as the effect of crumpling increases. Crumpling effects can be reduced by placing the antenna in the flatter regions of the body [13].

The effect of wetness on the antenna's performance has also been analyzed. When compared to measurement in dry conditions, in wet conditions, 5.13% frequency detuning is observed

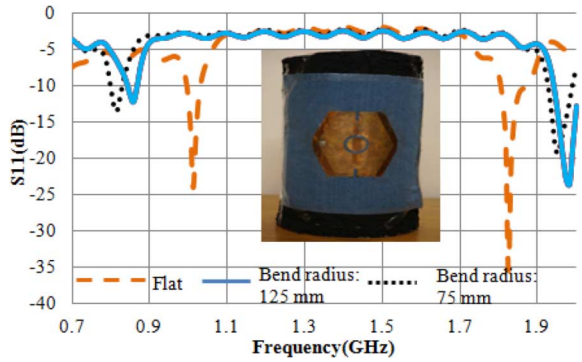

Fig. 9. Reflection coefficient characteristics of x-bent dual-band antenna.

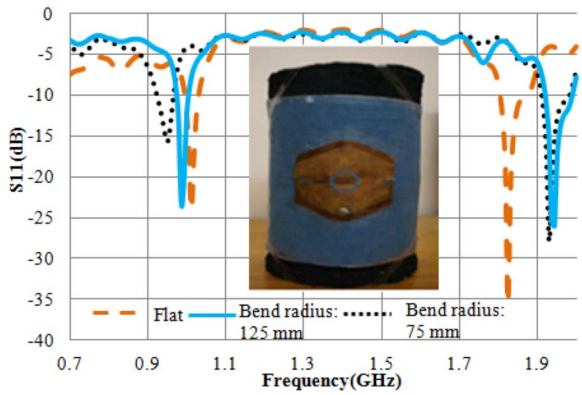

Fig. 10. Reflection coefficient characteristics of y-bent dual-band antenna.

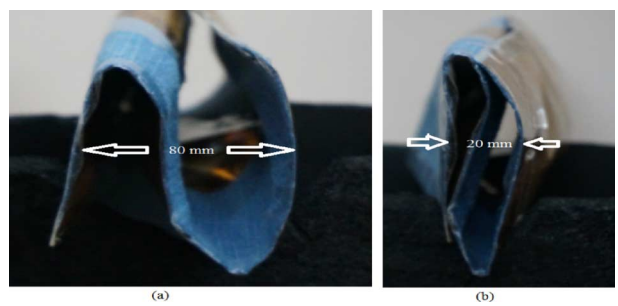

Fig. 11. (a) Slight crumple. (b) Severe crumple.

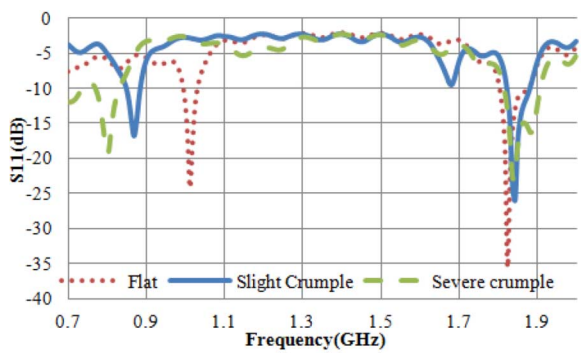

Fig. 12. Reflection coefficient characteristics of the dual-band antenna under different crumpling conditions.

in the lower band. In the upper band, 7.04% frequency detuning is observed.

The amount of electromagnetic radiation absorbed by the body tissues can be found by evaluating the specific absorption rate (SAR). The simplified three-layered rectangular body

TABLE II
THICKNESS, PERMITTIVITY, LOSS TANGENT, AND DENSITY OF THE THREE-LAYERED RECTANGULAR BODY MODEL AT 900 MHZ [16]

LAYER	THICKNESS (mm)	ε_r	LOSS TANGENT	DENSITY (Kg/m^3)
Skin	0.4	41.4	0.418	1100
Fat	30	5.46	0.186	1100
Muscle	69.6	55.0	0.342	1040

TABLE III
SAR VALUES AT VARIED DISTANCES OF ANTENNA FROM BODY TISSUES

Distance of separation	SAR(W/Kg)		Directivity (dBi)	
	900 MHz	1800 MHz	900 MHz	1800 MHz
$0.01\lambda_0$	0.00066	0.00237	8	4.6
$0.02\lambda_0$	0.00057	0.00198	8	4.6
$0.03\lambda_0$	0.00046	0.00162	8.033	4.6
$0.04\lambda_0$	0.00043	0.00132	8.1	4.7
$0.05\lambda_0$	0.00042	0.00109	8.1	4.7
$0.06\lambda_0$	0.00040	0.00092	8.1	4.7
$0.07\lambda_0$	0.00039	0.00079	8.1	4.7

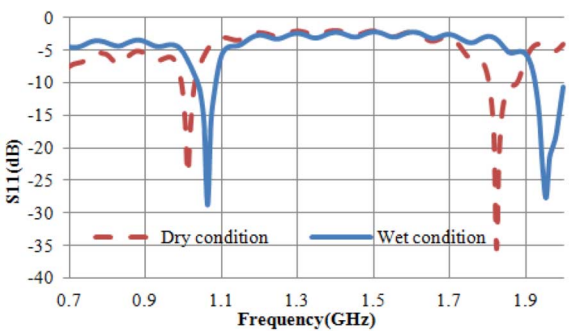

Fig. 13. Reflection coefficient characteristics of the dual-band antenna under dry and wet conditions.

model is chosen for our study since it was found to give good agreement with measurements. The thickness, permittivity (ε_r), loss tangent, and density of skin, fat, and muscle considered in this model are given in Table II.

In Table III, the mass averaged SAR (10 g) is estimated for distances varying from $0.01\lambda_0$ to $0.07\lambda_0$ between body tissue and antenna. The values of λ_0 and all the above parameters have been defined at 900 MHz [16]. According to International Electrotechnical Commission (IEC) standards, SAR limit is 2 W/Kg averaged over the 10 g of tissue. In both the bands, for varying distances of separation, SAR values obtained lies within the limits.

Another analysis, keeping the overall thickness as 100 mm and varying the depth of each layer is presented in Table IV. These analyses throw light on placement and positioning of wearable antennas, when they are modeled for any particular application. In this analysis also, SAR values lie within the IEC limits.

IV. CONCLUSION

In this letter, the design of a robust dual-band wearable antenna has been presented. The antenna exhibits satisfactory performance in both GSM-900 and 1800 bands.

TABLE IV
SAR VALUES FOR VARYING THICKNESS OF INDIVIDUAL LAYERS

Thickness(mm)			SAR (W/Kg)		Directivity (dBi)	
Skin	Fat	Muscle	900 MHz	1800 MHz	900 MHz	1800 MHz
0.4	0	99.6	0.0011	0.0034	8.2	7.5
0.4	15	84.6	0.0007	0.0028	8	7.5
0.4	30	69.6	0.0006	0.0023	8	7.6
2.6	0	97.6	0.0010	0.0035	8.2	7.5
2.6	15	82.4	0.0007	0.0027	8.1	7.6
2.6	30	67.4	0.0006	0.0011	8	7.7

As the given antenna is handmade, it is simple and cost-effective. Bending, crumpling, wetness, and on-body measurements have been done to validate the structure. SAR calculation is also done, and it is clear from Tables III and IV that the value lies well below the acceptable limit.

REFERENCES

[1] S. Sankaralingam and B. Gupta, "Determination of dielectric constant of fabric materials and their use as substrates for design and development of antennas for wearable applications," *IEEE Trans. Instrum. Meas.*, vol. 59, no. 12, pp. 3122–3130, Dec. 2010.
[2] S. Zhu and R. Langley, "Dual-band wearable textile antenna on an EBG substrate," *IEEE Trans. Antennas Propag.*, vol. 57, no. 4, pp. 926–935, Apr. 2009.
[3] S. Nikolaou, G. E. Ponchak, J. Papapolerou, and M. M. Tentzeris, "Conformal double exponentially tapered slot antenna (DETSA) on LCP for UWB application," *IEEE Trans. Antennas Propag.*, vol. 54, no. 6, pp. 1663–1668, Jun. 2006.
[4] M. A. R. Osman, M. K. A. Rahim, M. Azfar, N. A. Samsuri, F. Zubir, and K. Kamardin, "Design, implementation and performance of ultra-wideband textile antenna," *Prog. Electromagn. Res. B*, vol. 27, pp. 307–327, 2011.
[5] T. Watanabe and H. Iwasaki, "Wearable finger dual-band antenna for BAN," in *Proc. IEEE-APS Top. Conf.*, 2012, pp. 51–54.
[6] B. Sanz-Izquierdo, F. Huang, and J. C. Batchelor, "Covert dual-band wearable button antenna," *Electron. Lett.*, vol. 42, pp. 668–670, 2006.
[7] A. Alomainy, Y. Hao, A. Owadally, C. G. Parini, Y. Nechayev, C. C. Constantinou, and P. S. Hall, "Statistical analysis and performance evaluation for on-body radio propagation with microstrip patch antennas," *IEEE Trans. Antennas Propag.*, vol. 55, no. 1, pp. 245–248, Jan. 2007.
[8] A. Alomainy, A. Sani, A. Rahman, J. G. Santas, and Y. Hao, "Transient characteristics of wearable antennas and radio propagation channels for ultrawideband body-centric wireless communications," *IEEE Trans. Antennas Propag.*, vol. 57, no. 4, pp. 875–884, Apr. 2009.
[9] K. Qian and X. Tang, "Compact LTCC dual-band circularly polarized perturbed hexagonal microstrip antenna," *IEEE Antennas Wireless Propag. Lett.*, vol. 10, pp. 1212–1215, 2011.
[10] M. Chen and C. Chen, "A compact dual-band GPS antenna design," *IEEE Antennas Wireless Propag. Lett.*, vol. 12, pp. 245–248, 2013.
[11] I. Locher, M. Klemm, T. Kirstein, and G. Troster, "Design and characterization of purely textile patch antennas," *IEEE Trans. Adv. Packag.*, vol. 29, no. 4, pp. 777–788, Nov. 2006.
[12] P. Salonen and Y. Rahmat-Samii, "Textile antennas: Effects of antenna bending on input matching and impedance bandwidth," *IEEE Aerosp. Electron. Syst. Mag.*, vol. 22, no. 12, pp. 18–22, Dec. 2011.
[13] Q. Bai, J. Rigelsford, and R. Langley, "Crumpling of microstrip antenna array," *IEEE Trans. Antennas Propag.*, vol. 61, no. 9, pp. 4567–4576, Sep. 2013.
[14] C. A. Balanis, *Antenna Theory: Analysis and Design*, 3rd ed. Hoboken, NJ, USA: Wiley, 2012.
[15] K. E. Wasife, "Power density and SAR in multi-layered life tissue at Global System Mobile (GSM) frequencies," *J. Electromagn. Anal. Appl.*, vol. 3, no. 8, pp. 328–332, 2011.
[16] S. S. Mhaske, G. A. Kulkarni, and R. L. Tayade, "SAR in life tissue at GSM frequencies," *Int. J. Adv. Res. Comput. Sci. Softw. Eng.*, vol. 2, no. 4, pp. 480–483, 2012.
[17] V. Hebelka, "Planar antennas in proximity of human body models," *Elektrorevenue*, vol. 3, no. 4, pp. 10–13, Dec. 2012.